The influence of backward wave transmission on quantitative ultrasonic evaluation using Lamb wave propagation

T. Liu
Department of Civil Engineering, The University of Queensland, Brisbane, Qld 4072, Australia

W. Karunasena
Department of Civil and Environmental Engineering, School of Engineering, James Cook University, Townsville, Qld 4811, Australia

S. Kitipornchai[a)]
Department of Civil Engineering, The University of Queensland, Brisbane, Qld 4072, Australia

M. Veidt
Department of Mechanical Engineering, The University of Queensland, Brisbane, Qld 4072, Australia

In view of the various novel quantitative ultrasonic evaluation techniques developed using Lamb wave propagation, the influence of an important related phenomenon, backward transmission, is investigated in this paper. Using the discrete layer theory and a multiple integral transform method, the surface displacement and velocity responses of isotropic plates and cross-ply laminated composite plates due to the Lamb waves excited by parabolic- and piston-type transmitting transducers are evaluated. Analytical expressions for the surface displacement and velocity frequency response functions are developed. Based on this a large volume of calculations is carried out. Through examining the characteristics of the surface displacement and velocity frequency response functions and, especially, the different propagation modes' contributions to them, the influence of the backward wave transmission related to quantitative ultrasonic nondestructive evaluation applications is discussed and some important conclusions are drawn. © *2000 Acoustical Society of America.* [S0001-4966(99)04212-5]

PACS numbers: 43.40.Dx, 43.35.Cg [CBB]

INTRODUCTION

In recent years, the use of Lamb wave propagation to develop modern quantitative ultrasonic evaluation techniques has attracted rapidly growing interest for various purposes, for example, quick inspection of long gas or petroleum pipe lines, evaluation of complex damage state of composite structures and even real-time monitoring of composite manufacturing processes. Consequently, a clear understanding of the characteristics of the wave propagation involved is very important for the interpretation of measurement results as well as for the further optimization of the corresponding measurement techniques.

There has been a considerable amount of investigation on general characteristics of Lamb wave propagation, for example, Refs. 1–8. However, investigation of an important phenomenon related to the Lamb wave propagation, namely, backward wave transmission, is still limited. Based on the frequency equation for isotropic plates or cylinders, some researchers such as Tolstoy *et al.*[9] first predicted the presence of backward wave motion in which phase and group velocities have opposite signs. This means that energy is carried in a direction opposite to the motion of the waves. Several years later Meitzler[10] reported his experimental observations to give evidence of this interesting prediction and also gave an interpretation by comparing the displacement

components, stress components, and the average energy-flux density for the forward and backward motions. After that, Torvik[11] reconfirmed the presence of backward wave motion for a limited range of frequency during his investigation of the reflection of an infinite train of waves from the free edge of an isotropic plate. He also found that there exists a critical frequency in the second mode (nonpropagating mode) well below the first cutoff frequency near which the wave reflection coefficient experiences a sharp resonance in amplitude.

Considering the abnormal properties discovered for backward wave transmission in isotropic plates, the influence of backward waves involved in some quantitative ultrasonic evaluation techniques such as acousto-ultrasonics or stress wave factor technique for composite laminates is considered in this paper. Using discrete layer theory and a multiple integral transform method, the surface displacement and velocity responses of isotropic plates and cross-ply composite laminated plates due to Lamb waves excited by contact-type transducers such as adhesively bonded piezoceramic transducers are evaluated. Analytical expressions for the surface displacement and velocity frequency response functions are developed. Based on this, numerical calculations are carried out to examine the influence of backward wave transmission related to ultrasonic nondestructive evaluation applications.

I. FORMULATION OF THE PROBLEM

Consider a transmitting transducer attached to the upper surface of a composite laminated plate of thickness h as

---
a)Electronic mail: e2kitip@brolga.uq.edu.au

Transmitting
Transducer

Composite plate

FIG. 1. The problem considered in this paper.

shown in Fig. 1. It is assumed that the surface displacement or velocity is to be measured at another position. A Cartesian coordinate system (x,y,z) with origin on the upper surface of the laminate is introduced. Each lamina is modeled as a transversely isotropic material. For simplicity, we confine our attention to cross-ply laminates with the three axes coinciding with the axes of orthotropy and a plane strain condition with the y axis being perpendicular to the plane. Then, in the absence of body forces, the basic governing equations for the ith lamina bounded by $z=z_i$ and $z=z_{i+1}$ are

$$\begin{Bmatrix} \sigma_{xx} \\ \sigma_{zz} \\ \sigma_{xz} \end{Bmatrix} = \begin{bmatrix} c_{11} & c_{13} & 0 \\ c_{13} & c_{33} & 0 \\ 0 & 0 & c_{55} \end{bmatrix} \begin{Bmatrix} \epsilon_{xx} \\ \epsilon_{zz} \\ \gamma_{xz} \end{Bmatrix}, \qquad (1)$$

$$\epsilon_{xx}=\frac{\partial u}{\partial x}, \quad \epsilon_{zz}=\frac{\partial w}{\partial z}, \quad \gamma_{xz}=\frac{\partial u}{\partial z}+\frac{\partial w}{\partial x}, \qquad (2)$$

$$\frac{\partial \sigma_{xx}}{\partial x}+\frac{\partial \sigma_{xz}}{\partial z}=\rho \frac{\partial^2 u}{\partial t^2}, \qquad (3a)$$

$$\frac{\partial \sigma_{xz}}{\partial x}+\frac{\partial \sigma_{zz}}{\partial z}=\rho \frac{\partial^2 w}{\partial t^2}, \qquad (3b)$$

$$\sigma_{zz}|_{z=0}=-p_1(x,t), \qquad (4a)$$

$$\sigma_{xz}|_{z=0}=-p_2(x,t), \qquad (4b)$$

where σ_{ij} and ϵ_{ij} are stress and strain components, respectively; u and w denote displacement components in x and z axis directions, respectively; c_{ij} and ρ are elements of the constitutive matrix and density of the ith lamina, respectively; t denotes the time variable; and $p_1(x,t)$ and $p_2(x,t)$ represent the distributed traction excited by the transmitting transducer.

An approximate approach called the stiffness method[12–14] or discrete layer method[15] is used to solve the above equations. The essence of the method is to divide the plate into a number of mathematical layers in the thickness direction so that the variation of the displacements through the thickness of each layer can be approximated by various polynomials using interpolation for some unknown displacements. Using the principle of virtual work, the differential equations of the wave motion in the plate can then be expressed in a form in which there is no differentiation with respect to the variable in the thickness direction.

Following the procedure described in Refs. 12–15, it is assumed that the plate, as shown in Fig. 1, is divided into N mathematical layers. For the ith layer, the vector of displacements at an arbitrary point denoted by $\mathbf{U}_i(x,z) = [u_i(x,z), w_i(x,z)]^T$ is expressed by a quadratic polynomial interpolation as

$$\mathbf{U}_i=(x,z)=\mathbf{N}\mathbf{q}_i, \qquad (5)$$

where the matrix $\mathbf{q}$, a displacement vector composed of the displacement vectors for the upper surface, the middle plane and the lower surface of the ith layer, and the matrix $\mathbf{N}$, the corresponding shape function, can be expressed as

$$\mathbf{q}_i^T=[\mathbf{U}_i^T|_{\eta=0},\mathbf{U}_i^T|_{\eta=1/2},\mathbf{U}_i^T|_{\eta=1}], \qquad (6)$$

$$\mathbf{N}=[2\eta^2-3\eta+1)\mathbf{I},(-4\eta^2+4\eta)\mathbf{I},(2\eta^2-\eta)\mathbf{I}], \qquad (7)$$

in which $\mathbf{I}$ is a 2×2 identity matrix and η is the normalized measure for the ith layer defined by

$$\eta=(z-z_{iu})/h_i, \qquad (8)$$

where z_{iu} and h_i are the z coordinate of the upper surface and the thickness of the ith layer, respectively.

Applying the principle of virtual work to the ith layer, we have

$$\delta\mathbf{q}_i^T\mathbf{T}_i=\delta\mathbf{q}_i^T\mathbf{S}_i+\int_{z_{iu}}^{z_{iu}+h_i}\delta\mathbf{U}_i^T(\rho_i\ddot{\mathbf{U}}_i-\mathbf{L}^\tau\sigma_i-\mathbf{f}_i)dz, \qquad (9)$$

with

$$\sigma_i^T=[\sigma_{xx},\sigma_{zz},\sigma_{xz}], \qquad (10a)$$

$$\mathbf{f}_i^T=[f_x,f_z], \qquad (10b)$$

$$\mathbf{S}_i^T=[-\sigma_{xz}|_{\eta=0},-\sigma_{zz}|_{\eta=0},0,0,\sigma_{xz}|_{\eta=1},\sigma_{zz}|_{\eta=1}], \qquad (10c)$$

$$\mathbf{T}_i^T=[p_{xz}|_{\eta=0},p_{zz}|_{\eta=0},p_{xz}|_{\eta=1/2},p_{zz}|_{\eta=1/2},$$
$$p_{xz}|_{\eta=1},p_{zz}|_{\eta=1}], \qquad (10d)$$

$$\mathbf{L}^T=\begin{bmatrix} \dfrac{\partial}{\partial x} & 0 & \dfrac{\partial}{\partial z} \\ 0 & \dfrac{\partial}{\partial z} & \dfrac{\partial}{\partial x} \end{bmatrix}, \qquad (10e)$$

where σ_i, $\mathbf{f}_i$, $\mathbf{S}_i$ and $\mathbf{T}_i$ represent the stress vector, the body force vector, the upper and lower interface traction vector, and the probable external load vector for the ith layer, respectively. Here p_{xz} and p_{zz} are the shear and normal external traction. ρ_i is its mass density. The symbol ''·'' indicates differentiation with respect to time.

Substituting Eqs. (5)–(7) into Eq. (9) and using the general relations among stresses, strains and displacements, the governing equation for the ith layer can be expressed as

$$\mathbf{M}^{(i)}\frac{\partial^2}{\partial t^2}\mathbf{q}_i+\left[-\mathbf{K}_1^{(i)}\frac{\partial^2}{\partial x^2}-\mathbf{K}_4^{(i)}\frac{\partial}{\partial x}+\mathbf{K}_6^{(i)}\right]\mathbf{q}_i=\mathbf{T}_i, \qquad (11)$$

where $\mathbf{M}^{(i)}$, $\mathbf{K}_1^{(i)}$, $\mathbf{K}_4^{(i)}$ and $\mathbf{K}_6^{(i)}$ and 6×6 matrices which are given in the Appendix (item 1). In the derivation of Eq. (11), it is assumed that no body forces exist.

In the same way, obtaining all the governing equations for the N layers, and then assembling them from the top layer to the bottom layer, the governing equation for the laminated plate can be finally expressed as

$$\mathbf{M}\frac{\partial^2}{\partial t^2}\mathbf{q}+\left[-\mathbf{K}_1\frac{\partial^2}{\partial x^2}-\mathbf{K}_4\frac{\partial}{\partial x}+\mathbf{K}_6\right]\mathbf{q}=\mathbf{T}, \qquad (12)$$

where $\mathbf{q}$, $\mathbf{T}$, $\mathbf{M}$, $\mathbf{K}_1$, $\mathbf{K}_4$, and $\mathbf{K}_6$ are the global matrices produced by assembling $\mathbf{q}_i$, $\mathbf{T}_i$, $\mathbf{M}^{(i)}$, $\mathbf{K}_1^{(i)}$, $\mathbf{K}_4^{(i)}$ and $\mathbf{K}_6^{(i)}$ ($i=1,2,3,...,N$), respectively.

In order to simplify the problem, as presented in Refs. 16 and 17 it is assumed that the pressure distribution between the transducer and the plate can be approximated by a piston distribution or a parabolic distribution. The contact pressure $p_i(x,t)$ exerted on the surface of the plate by the transducer can therefore be expressed as

$$p_i(x,t)=[\mathrm{H}(x+a)-\mathrm{H}(x-a)]D(x,a)p_i(t), \quad i=1,2,$$
(13)

in which a is the aperture of the transmitting transducer, $\mathrm{H}(x)$ stands for the Heaviside function, $p_i(t)(i=1,2)$ are the normal and tangential forces exerted on the plate by the transmitting transducer, and $D(x,a)$ is the contact pressure distribution function which for a piston distribution is defined as

$$D(x,a)=\begin{cases} 1, & |x|\leqslant a, \\ 0, & |x|>a, \end{cases}$$
(14)

and for a parabolic distribution as

$$D(x,a)=\begin{cases} \frac{3}{2}[1-(x/a)^2], & |x|\leqslant a, \\ 0, & |x|>a. \end{cases}$$
(15)

The resultant force is the same in both cases.

Expressing the above contact pressure in the form of the external load vector given in (12) yields to

$$\mathbf{T}=p_1(x,t)\mathbf{C}_1+p_2(x,t)\mathbf{C}_2$$
(16)

where $\mathbf{C}_1$ and $\mathbf{C}_2$ are constant vectors of length $2(2N+1)$, which are given by

$$\mathbf{C}_1^T=[0,1,0,0,...,0],$$
(17a)

$$\mathbf{C}_2^T=[1,0,0,0,...,0].$$
(17b)

II. FREQUENCY DOMAIN SOLUTION AND INVERSION

Applying the Fourier time transform and spatial transform defined as

$$\bar{g}(x,\omega)=\int_0^\infty g(x,t)e^{-i\omega t}dt,$$
(18)

$$\tilde{g}(\kappa,t)=\int_{-\infty}^{+\infty} g(x,t)e^{-i\kappa x}dx,$$
(19)

to Eqs. (12) on t and x, respectively, we have

$$(\kappa^2\mathbf{K}_1-i\kappa\mathbf{K}_4+\mathbf{K}_6-\omega^2\mathbf{M})\tilde{\bar{\mathbf{q}}}=\tilde{\bar{\mathbf{T}}}.$$
(20)

Solving the above equation yields to[18]

$$\tilde{\bar{\mathbf{q}}}=i\sum_{m=1}^{2M} \frac{\boldsymbol{\psi}_{ml}^T\tilde{\bar{\mathbf{T}}}}{(\kappa-\kappa_m)\boldsymbol{\psi}_m^T\mathbf{R}\boldsymbol{\varphi}_m}\boldsymbol{\varphi}_{mu},$$
(21)

where $M=2(2N+1)$ and $\kappa_m=i\lambda_m$. φ_m, ψ_m and λ_m ($m=1$ to $2M$) are the eigenvectors and eigenvalues of the following two characteristic equations:

$$(\mathbf{Q}-\lambda\mathbf{R})\varphi=\mathbf{0},$$
(22a)

$$(\mathbf{Q}^T-\lambda\mathbf{R}^T)\psi=\mathbf{0}$$
(22b)

in which

$$\mathbf{Q}=\begin{bmatrix} \mathbf{0} & \mathbf{I} \\ \omega^2\mathbf{M}-\mathbf{K}_6 & -\mathbf{K}_4 \end{bmatrix},$$
(23a)

$$\mathbf{R}=\begin{bmatrix} \mathbf{I} & \mathbf{0} \\ \mathbf{0} & -\mathbf{K}_1 \end{bmatrix},$$
(23b)

where $\mathbf{I}$ is an identity matrix of the same dimension as $\mathbf{M}$, $\mathbf{K}_1$, $\mathbf{K}_4$, and $\mathbf{K}_6$. φ_{mu} and ψ_{ml} are the upper and lower halves of the eigenvectors φ_m and ψ_m, respectively.

Substituting Eqs. (13)–(15) to Eq. (16) and then applying the Fourier transformations (18) and (19) to resulting equation on variable t and x, respectively, yields

$$\tilde{\bar{\mathbf{T}}}=\bar{p}_1(\omega)I(\kappa)\mathbf{C}_1+\bar{p}_2(\omega)I(\kappa)\mathbf{C}_2,$$
(24)

in which $I(\kappa)$ is given as for piston-type force distribution,

$$I(\kappa)=i[e^{i\kappa(x-a)}-e^{i\kappa(x+a)}]/\kappa, \quad x>a,$$
(25a)

and for parabolic-type force distribution,

$$I(\kappa)=3[(i-\kappa a)e^{i\kappa(x-a)}-(i+\kappa a)e^{i\kappa(x+a)}]/(\kappa^3 a^2)],$$
$$x>a.$$
(25b)

Applying the inverse Fourier spatial transform of Eq. (19) to Eqs. (21) and (24), we have

$$\bar{\mathbf{q}}(x)=\bar{\mathbf{q}}_1+\bar{\mathbf{q}}_2$$
(26)

with

$$\bar{\mathbf{q}}_j=\frac{i}{2\pi}\bar{p}_j(\omega)\int_{-\infty}^\infty \sum_{m=1}^{2M} \frac{I(\kappa)\boldsymbol{\psi}_{ml}^T\mathbf{C}_j}{(\kappa-\kappa_m)\boldsymbol{\psi}_m^T\mathbf{R}\boldsymbol{\varphi}_m}\boldsymbol{\varphi}_{mu}d\kappa,$$
$$j=1,2.$$
(27)

Considering the real measurements, from the general displacement expression (26), the frequency domain solution of the top surface displacement $w(x,0,t)$ and velocity $V(x,0,t)$ of the plate are expressed as

$$\bar{w}(x,0,\omega)=G_1(\omega)\bar{p}_1(\omega)+G_2(\omega)\bar{p}_2(\omega),$$
(28)

$$\bar{V}(x,0,\omega)=-i\omega G_1(\omega)\bar{p}_1(\omega)-i\omega G_2(\omega)\bar{p}_2(\omega),$$
(29)

in which

$$G_j(\omega)=\frac{i}{2\pi}\int_{-\infty}^\infty \sum_{m=1}^{2M} \frac{(\boldsymbol{\psi}_{ml}^T\mathbf{C}_j)(\boldsymbol{\varphi}_{mu}^T\mathbf{C}_1)}{(\kappa-\kappa_m)\boldsymbol{\psi}_m^T\mathbf{R}\boldsymbol{\varphi}_m}I(\kappa)d\kappa,$$
$$j=1,2,$$
(30a)

$$H_j(\omega)=-i\omega G_j(\omega), \quad j=1,2.$$
(30b)

Applying the contour integration technique[19] to Eq. (30a), $G_j(\omega)$ can be simplified as

TABLE I. Engineering constants of two types of plates used in the calculation.

Material	E_1 (Gpa)	E_2 (Gpa)	G_{12} (Gpa)	G_{13} (Gpa)	G_{23} (Gpa)	ν_{12}	ρ (Kg/m^3)
Aluminum	73	73	28.077	28.077	28.077	0.3	2770
Glass/epoxy	38.612	8.274	4.137	4.137	3.448	0.26	1800

$$G_j(\omega) = -\sum_{m=1}^{M_i} \frac{(\boldsymbol{\psi}_{ml}^T \mathbf{C}_j)(\boldsymbol{\varphi}_{mu}^T \mathbf{C}_1)}{\boldsymbol{\psi}_m^T \mathbf{R} \boldsymbol{\varphi}_m} I(\kappa_m)$$
$$-\sum_{m=1}^{M_c} \frac{(\boldsymbol{\psi}_{ml}^T \mathbf{C}_j)(\boldsymbol{\varphi}_{mu}^T \mathbf{C}_1)}{\boldsymbol{\psi}_m^T \mathbf{R} \boldsymbol{\varphi}_m} I(\kappa_m), \quad j=1,2, \quad (31)$$

where M_r is the number of the real wave modes with positive group velocities, i.e., carrying energy towards the positive x-axis direction, and M_c is the number of complex wave modes corresponding to the κ_m with Im$(\kappa_m) > 0$.

In view of Eqs. (28) and (29) $G_1(\omega)$, $G_2(\omega)$ and $H_1(\omega)$, $H_2(\omega)$ can be called the displacement and velocity frequency response functions corresponding to the normal traction and shear traction excited by the transmitting transducer.

Applying the inverse Fourier time transformation to the frequency domain solution Eqs. (28) and (29), the time domain solution of the surface displacement and velocities can be expressed as

$$w(x,0,t) = \int_{-\infty}^{\infty} [G_1(\omega)\bar{p}_1(\omega) + G_2(\omega)\bar{p}_2(\omega)] e^{i\omega t} d\omega, \tag{32a}$$

$$V(x,0,t) = \int_{-\infty}^{\infty} [H_1(\omega)\bar{p}_1(\omega) + H_2(\omega)\bar{p}_2(\omega)] e^{i\omega t} d\omega. \tag{32b}$$

The computation of Eqs. (32a) and (32b) can be carried out using the fast Fourier transform (FFT) technique.

III. THE SOLUTION BASED ON SIMPLIFED THEORIES

Although simplified plate theories such as the classical plate theory and the Mindlin plate theory cannot be used to examine backward wave transmission, they are still useful for result comparison or program check in low-frequency regions. In this section, the corresponding solution based on the Mindlin plate theory is presented.

Using the same coordinate system as above, the equations of the motion for the plate in a state of plane strain parallel to the x-z plane are

$$kA_{55}\left(\frac{\partial \varphi_x}{\partial x} + \frac{\partial^2 w}{\partial w^2}\right) + p_1 = \rho h \frac{\partial^2 w}{\partial t^2}, \tag{33a}$$

$$D_{11}\frac{\partial^2 \varphi_x}{\partial x^2} - kA_{55}\left(\varphi_x + \frac{\partial w}{\partial x}\right) = \frac{\rho h^3}{12} \frac{\partial^2 \varphi_x}{\partial t^2}, \tag{33b}$$

where w is the transverse displacement; φ_x is the rotation of the plane section perpendicular to the x axis; p_1 is seen in Eq. (13); $k(=\pi^2/12)$ is a shear correction factor; and A_{55} and D_{11} are the plate transverse-shear and plate bending ri-

gidities, respectively. A_{55} and D_{11} are given by

$$A_{55} = \sum_{k=1}^{N} \bar{Q}_{55}^{(k)}(\bar{z}_{k+1} - \bar{z}_k), \tag{34a}$$

$$D_{11} = \frac{1}{3}\sum_{k=1}^{N} \bar{Q}_{11}^{(k)}(\bar{z}_{k+1}^3 - \bar{z}_k^3), \tag{34b}$$

$$\bar{Q}_{55}^{(k)} = Q_{55}^{(k)}\cos^2\theta_k + Q_{44}^{(k)}\sin^2\theta_k, \tag{34c}$$

$$\bar{Q}_{11}^{(k)} = Q_{11}^{(k)}\cos^4\theta_k + Q_{22}^{(k)}\sin^4\theta_k, \tag{34d}$$

$$Q_{11}^{(k)} = E_1^{(k)}/(1 - \nu_{12}^{(k)}\nu_{21}^{(k)}), \tag{34e}$$

$$Q_{22}^{(k)} = \nu_{12}^{(k)}E_2^{(k)}/(1 - \nu_{12}^{(k)}\nu_{21}^{(k)}), \tag{34f}$$

$$Q_{44}^{(k)} = G_{23}^{(k)}, \tag{34g}$$

$$Q_{55}^{(k)} = G_{13}^{(k)}, \tag{34h}$$

$$\nu_{21}^{(k)} = \nu_{12}^{(k)}E_2^{(k)}/E_1^{(k)}, \tag{34i}$$

where $\bar{z}_k = z_k - h/2$, $Q_{ii}^{(k)}$ ($i=1,2,4,5$) is the material stiffness constant of kth layer, θ_k is the angle between the fiber direction of kth layer and the x axis (0 or 90 degrees), and $E_1^{(k)}$, $E_2^{(k)}$, $G_{13}^{(k)}$, $G_{23}^{(k)}$, and $\nu_{12}^{(k)}$ are the engineering constants for the kth layer.

Based on Eqs. (33a), (33b) and (13)–(15), using a similar Fourier transformation procedure, the solution corresponding to Eq. (28) can be obtained as follows:

For parabolic source,

$$\bar{w}(x,0,\omega) = \bar{p}_1(\omega)[\mu_{11}e^{-i\kappa_1(x-a)} + \mu_{12}e^{i\kappa_1(x+a)} + \mu_{21}e^{-\gamma(x-a)} + \mu_{22}e^{-\gamma(x+a)}], \quad |\omega| < \omega_c, \tag{35a}$$

$$\bar{w}(x,0,\omega) = \bar{p}_1(\omega)[\mu_{11}e^{-i\kappa_1(x-a)} + \mu_{12}e^{-i\kappa_1(x+a)} + \mu_{21}e^{-i\kappa_2(x-a)} + \mu_{22}e^{-i\kappa_2(x+a)}], \quad |\omega| \geq \omega_c. \tag{35b}$$

For piston source,

$$\bar{w}(x,0,\omega) = \bar{p}_1(\omega)\{\nu_1[e^{-i\kappa_1(x-a)} - e^{-i\kappa_1(x+a)}] + \nu_2[e^{-\gamma(x-a)} - e^{-\gamma(x+a)}]\}, \quad |\omega| < \omega_c, \tag{36a}$$

$$\bar{w}(x,0,\omega) = \bar{p}_1(\omega)\{\nu_1[e^{-i\kappa_1(x-a)} - e^{-i\kappa_1(x+a)}] + \nu_2[e^{-i\kappa_2(x-a)} - e^{i\kappa_2(x+a)}]\}, \quad |\omega| \geq \omega_c, \tag{36b}$$

where the coefficients μ_{ij}, ν_i ($ij=1,2$) are given in the Appendix (item 2), and the cutoff frequency ω_c and wave number κ_1 and κ_2 are given by
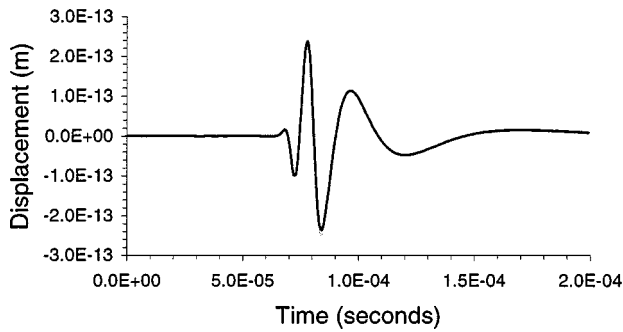
FIG. 2. Time history of the surface displacement evaluated by the discrete layer theory (thin line) and Mindlin plate theory (thick line) (composite plate 0/90/0, $h=2$ nm, $x=100$ mm; parabolic source $a=5$ mm, $f_0=0.125$ MHz, $n_0=2$; $f_c=0.368$ MHz).

$$\kappa_1 = \left[\frac{1}{2} \left(\frac{1}{c_0^2} + \frac{1}{c_s^2} \right) \omega^2 + \sqrt{ \frac{1}{4} \left(\frac{1}{c_0^2} - \frac{1}{c_s^2} \right)^2 \omega^4 + \frac{1}{c_0^2 \alpha^2} \omega^2 } \right]^{1/2},$$

$$|\omega| < \infty, \tag{37}$$

$$\kappa_2 = i\gamma \quad \text{for } |\omega| \leq \omega_c, \tag{38a}$$

$$\kappa_2 = \left[\frac{1}{2} \left(\frac{1}{c_0^2} + \frac{1}{c_s^2} \right) \omega^2 - \sqrt{ \frac{1}{4} \left(\frac{1}{c_0^2} - \frac{1}{c_s^2} \right)^2 \omega^4 + \frac{1}{c_0^2 \alpha^2} \omega^2 } \right]^{1/2}$$

$$\text{for } |\omega| > \omega_c, \tag{38b}$$

in which

$$\gamma = \left[\sqrt{ \frac{1}{4} \left(\frac{1}{c_0^2} - \frac{1}{c_s^2} \right)^2 \omega^4 + \frac{1}{c_0^2 \alpha^2} \omega^2 } \right.$$
$$\left. - \frac{1}{2} \left(\frac{1}{c_0^2} + \frac{1}{c_s^2} \right) \omega^2 \right]^{1/2}, \tag{39a}$$

$$c_0 = \sqrt{\frac{12 D_{11}}{\rho h^3}}, \tag{39b}$$

$$c_s = \sqrt{\frac{A_{55} k}{\rho h}}, \tag{39c}$$

$$\alpha = \frac{h}{\sqrt{12}}, \tag{39d}$$

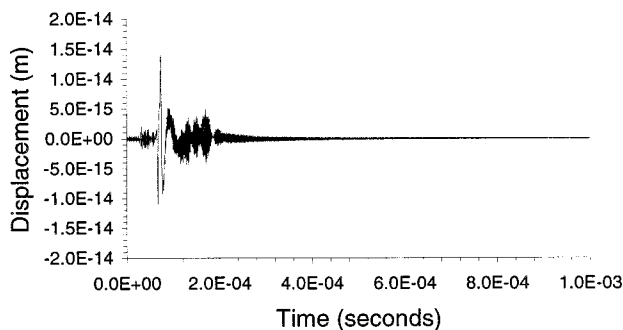$$\omega_c = \sqrt{\frac{12 A_{55} k}{\rho h^3}}. \tag{39e}$$

FIG. 3. Time history of the surface displacement evaluated by the discrete layer theory (composite plate 0/90/0, $h=2$ mm, $x=100$ mm; parabolic source $a=5$ mm, $f_0=0.4$ MHz, $n_0=2$; $f_c=0.368$ MHz).
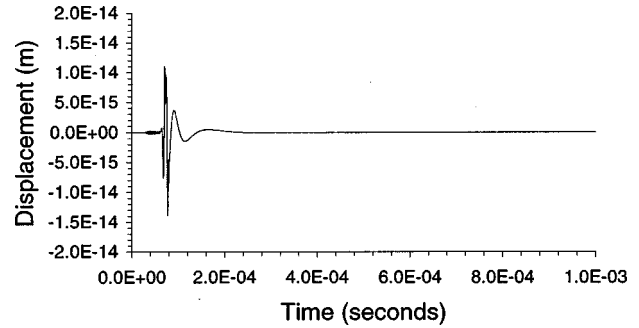

FIG. 4. Time history of the surface displacement evaluated by the Mindlin plate theory (composite plate 0/90/0, $h=2$ mm, $x=100$ mm; parabolic source $a=5$ mm, $f_0=0.4$ MHz, $n_0=2$; $f_c=0.368$ MHz).

Similarly, applying the inverse Fourier time transformation to Eqs. (35a), (35b), (36a), and (36b), the time domain solutions of the surface displacement can be obtained.

IV. NUMERICAL RESULTS AND DISCUSSION

In this section, based on the above analytical formulations, some numerical calculations are carried out to examine the characteristics of backward wave motion and its influence on the surface displacement and velocity responses of the plate interrogated by the transmitting transducer.

Two types of materials were used in the calculations. One is an isotropic aluminum, and the other is a glass/epoxy composite. Their engineering material constants are given in Table I.

Also, in the calculation the input pulse used is the delayed sine pulse with Haning window, i.e.,

$$p_i(t) = \begin{cases} 0.5 [1 - \cos(2\pi f_0 t/n_0)] \cos(2\pi f_0 t), & t \leq n_0/f_0, \\ 0, & t > n_0/f_0, \end{cases} \tag{40}$$

where f_0 is the central frequency and n_0 is the number of periods.

As a program check, the surface displacement response of a composite laminate ($0°/90°/0°$) of thickness $h=2$ mm due to parabolic source pulse is evaluated by both the discrete layer theory and the Mindlin plate theory. Figure 2 shows both results for low-frequency input (the dominant frequency is 0.125 MHz). It is seen that they are very close to each other. Using the same program the results for relatively high-frequency input (the dominant frequency is 0.4 MHz) are evaluated by the two theories in Figs. 3 and 4, respectively. For this frequency range the results of the two analysis models show some differences. It is evident that the above results are reasonable, considering the approximation involved in the Mindlin plate theory. This demonstrates, to some extent, the validity of the analysis and the computer program. Based on this, the backward wave motion characteristics and its influence are examined in the following paragraphs.

The dispersion curves for the aluminum plate which can be obtained by solving characteristic equation (22a) or (22b),
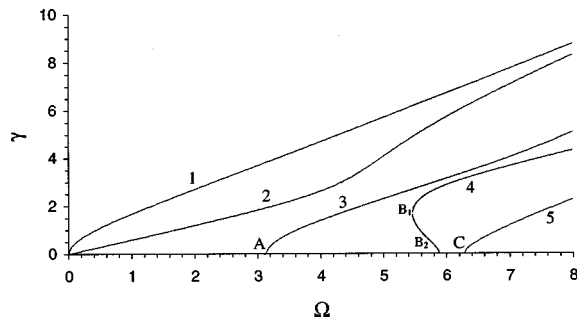
FIG. 5. The dispersion curves of normalized frequency $\Omega = \omega h / c_s$ and normalized wave number $\gamma = \kappa h$ for an isotropic plate with Poisson's ratio $\nu = 0.3$.

are shown in Fig. 5. Since the wave number κ and the frequency ω have been normalized by $\Omega = \omega h / c_s$ and $\gamma = \kappa h$, respectively, where $c_s = \sqrt{G/\rho}$ with G and ρ being the shear modulus and the mass density, the dispersion curves obtained are valid for a wide range of isotropic plate cases as long as the Possion's ratio $\nu = 0.3$. In this figure, the backward wave branch is marked by $B_1 B_2$, in which the phase and group velocities are of opposite sign. It is necessary to point out that branch $B_1 B_2$ here should be understood as its image with respect to the Ω axis, which has a positive group velocity. Additionally, for simplicity B_1 and B_2 are called the beginning and end points of the backward wave region in this paper, although B_2 is usually called the cutoff frequency of the second symmetric real branch.

Referring to Eq. (28), Fig. 6 shows the variation in amplitude of the normalized displacement frequency response function $G_1(\omega)$ at two different surface points due to a normal pressure pulse transmitted by a parabolic source. There are two singularities at the beginning and end points of the backward wave region, while at their two neighboring points A and C which are the first and second cutoff frequencies of antisymmetric modes there exist no singularities. This phenomenon is useful for understanding the peaks in the corresponding amplitude spectrum of a response signal when the input frequency covers this region. Additionally, it can also be seen that in relatively high-frequency cases, the displacement frequency response function has larger amplitude within and near the backward wave region. This means in such regions Lamb waves can carry more energy. However,
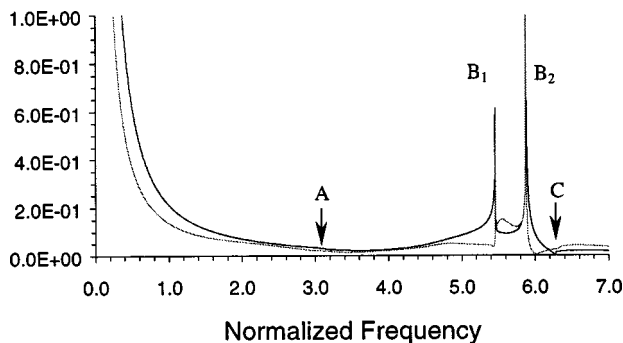
since there are several wave branches which have different group velocities, such regions will therefore cause more dispersion or distortion of time domain signals if many wave modes are involved in measurements.

Under the same condition as in Fig. 6, the displacement frequency response function $G_2(\omega)$ due to a shear force source is examined in Fig. 7. It is found that, (1) at the beginning point of the backward wave region there still exists a singularity, and near this singularity point $G_2(\omega)$ still has higher amplitude, while at the end point there is only a little discontinuity. (2) At the points A and C which correspond to the cutoff frequencies of the second and third antisymmetric real branches, there occur small discontinuities. (3) Compared with $G_1(\omega)$, $G_2(\omega)$ is of smaller amplitude in the low-frequency region.

In order to further understand the influence of backward wave transmission at the observation point farther away from the transmitting transducer, the contributions of different real branches (i.e., the propagation modes) to the displacement frequency response function due to a normal pressure pulse transmitted by a parabolic source are shown in Fig. 8. The figure clearly shows that the backward wave branch causes two singularities at its beginning and end points and, compared with other branches in this frequency region it has apparently higher amplitude. This implies that the backward wave branch makes the major contribution to the peak area of the overall frequency spectrum when multiple wave modes are excited as shown in Fig. 6. In other words, the
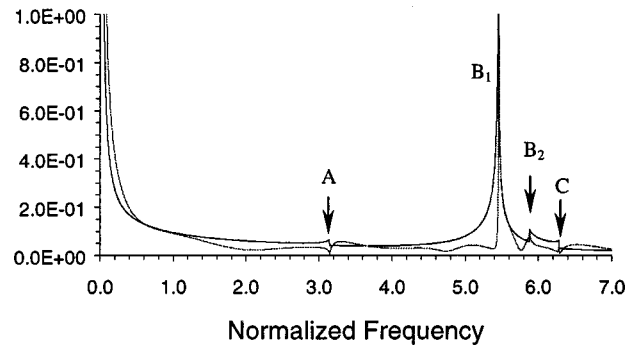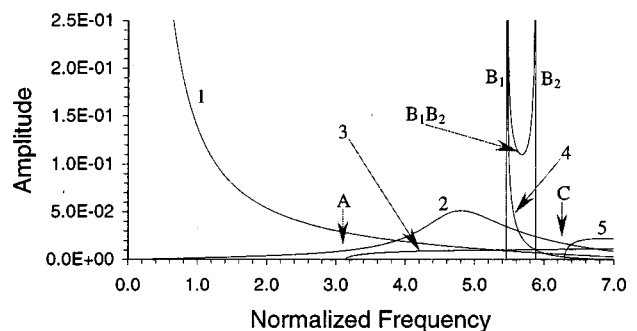

FIG. 7. Surface displacement frequency response function ($GG_2/h \sim \omega h / c_s$) at two different points $x/h = 0.833$ (solid line) and 8.33 (dashed line) on an isotropic plate ($\nu = 0.3$) due to a shear force pulse transmitted by a parabolic source ($a/h = 0.5$).

FIG. 6. Surface displacement frequency response ($GG_1/h \sim \omega h / c_s$) at two different points $x/h = 0.833$ (solid line) and 8.33 (dashed line) on an isotropic plate ($\nu = 0.3$) due to a normal pressure pulse transmitted by a parabolic source ($a/h = 0.5$).

FIG. 8. Contributions of different real branches to the surface displacement frequency response function ($GG_1/h \sim \omega h / c_s$) at $x/h = 8.33$ on an isotropic plate ($\nu = 0.3$) due to a normal pressure pulse transmitted by a parabolic source ($a/h = 0.5$) (referring to Fig. 5).
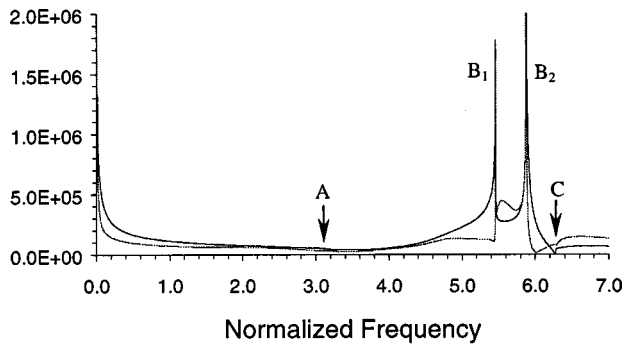
FIG. 9. Surface velocity frequency response function ($GH_1/h \sim \omega h/c_s$) at two different points $x/h = 0.833$ (solid line) and 8.33 (dashed line) on an isotropic plate ($\nu = 0.3$) due to a normal pressure pulse transmitted by a parabolic source ($a/h = 0.5$).

FIG. 11. The dispersion curves of normalized frequency $\Omega = \omega h/\sqrt{G_{12}/\rho}$ and normalized wave number $\gamma = \kappa h$ for a glass/epoxy composite laminated plate [(0/90/0/90/0)s].

peak area of the overall spectrum is dominated by the backward wave mode. But, unfortunately, since the backward wave mode has much smaller wave number, i.e., much longer wave length (see Fig. 5) than other branches in this region, the backward wave propagation will decrease the overall sensitivity for damage detection in this frequency region. On the other hand, however, if the damage size concerned can be compared with the wave length of the backward wave or long distance wave interrogation is required, then the use of the single backward wave mode which can be achieved by interdigital transducers could probably have some advantages because it appears that the backward wave can be excited more efficiently.

The contributions of different real branches to the displacement frequency response function $G_1(\omega)$ due to a normal pressure pulse transmitted by a piston-type source have also been examined. Compared with Fig. 8, it is found that there is no apparent difference in the backward wave contribution between the parabolic and piston source cases.

In consideration of the common use of the noncontact Doppler laser vibrometer system to measure surface velocity,[20] in Fig. 9 the frequency response function of surface velocities $H_1(\omega)$ [see Eq. (29)] due to a normal pressure pulse transmitted by a parabolic source is shown, and in Fig. 10 different real branches' contributions to $H_1(\omega)$ for the point farther away from the source are illustrated. The same behavior induced by the backward wave transmission in the
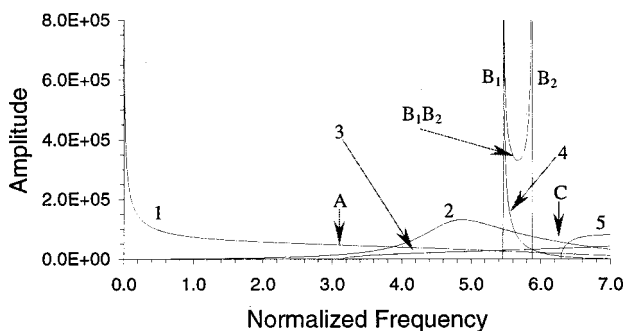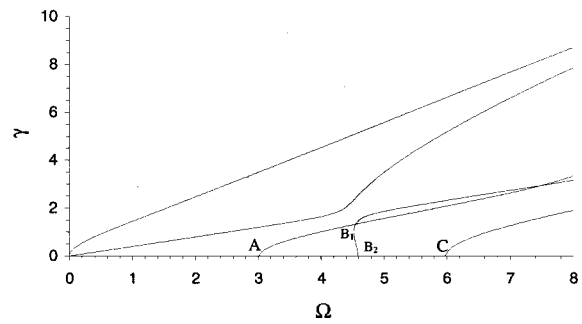
case of surface displacement measurement can be found in velocity measurement. So the above discussions about the backward transmission measured by surface displacement also applies to the cases for velocity measurement. However, it is of interest to note that $H_1(\omega)$ has relatively lower amplitude than $G_1(\omega)$ in the low frequency region.

Figure 11 shows the normalized dispersion curves of a glass/epoxy composite plate laminated as (0°/90°/0°/90°/0°)s. In Fig. 12 its surface velocity frequency response function due to normal pressure pulses transmitted by a parabolic-type transducer is presented. It can be seen that no matter whether the plate is isotropic or orthotropic, the behavior caused by the backward wave transmission is similar. This is because the characteristics of the dispersion curves in both cases are similar.

V. CONCLUSION

In this paper, in recognition of the various quantitative ultrasonic evaluation techniques using Lamb waves propagation, the influence of backward wave transmission in isotropic plates and cross-ply laminated composite plates has been investigated. Using the discrete layer theory, the surface displacement and velocity responses due to the Lamb waves excited by transmitting transducers have been evaluated. Expressions of the surface displacement and velocity frequency response functions have been presented. For comparison, analytical results using the Mindlin plate theory have also been developed. Based on the analytical results numerical
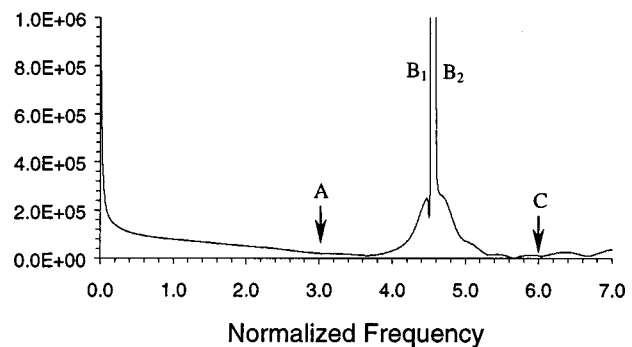

FIG. 10. Contributions of different real branches to the surface velocity frequency response function ($GH_1/h \sim \omega h/c_s$) at $x/h = 0.833$ on an isotropic plate ($\nu = 0.3$) due to a normal pressure pulse transmitted by a parabolic source ($a/h = 0.5$) (referring to Fig. 5).

FIG. 12. Surface velocity frequency response function ($GH_1/h \sim \omega h/\sqrt{G_{12}/\rho}$) at point $x/h = 10$ on a glass/epoxy composite laminated plate [(0/90/0/90/0)s] due to a normal pressure pulse transmitted by a parabolic source ($a/h = 1$).

calculations were carried out to check the validity of the analysis and then to examine the behavior of the backward wave transmission. The following conclusions have been drawn:

(1) For a moderately thick plate or relatively high-frequency input pulses, there exists apparent backward wave transmission. It is essential to consider its influence in this frequency regime for the development of guided wave quantitative nondestructive evaluation techniques.

(2) At the beginning point of the backward wave region, the normal surface displacement and velocity frequency response functions have a singularity no matter whether the transducer transmits normal forces or shear forces, while at the end point a singularity occurs only for the case of a normal pressure source. This is important for the interpretation of peak points in the output frequency spectra.

(3) The backward wave branch carries much more energy than other branches in the backward wave frequency regime. This implies that the backward transmission, on one hand, will decrease the resolution of damage detection if the ultrasonic techniques involve multiple wave modes and their input frequency cover this region since the corresponding wave lengths are large. On the other hand, however, it could be an advantage for some single-wave-mode related ultrasonic evaluation techniques.

(4) The surface displacement and velocity frequency response functions have the same behavior in the backward wave frequency region, e.g., relatively higher amplitude, but in the low-frequency region, the former has relatively higher amplitude than the latter.

(5) The presented figures for the different real branches' contributions to the surface displacement and velocity frequency response functions are of significance for selecting optimized input frequency regimes and the interpretation of the corresponding measurement results.

(6) It should be noted that in the analysis presented in this paper no damping was introduced, so the conclusions obtained above are only valid for structures with no or only small damping. For highly damped structural systems, it is necessary to take into account the damping influence when similar investigations are carried out.

APPENDIX

(1) The matrices in Eq. (11) for the ith layer are

$$\mathbf{M}^{(i)} = \frac{1}{30} h_i \rho_i \begin{bmatrix} 4\mathbf{I} & 2\mathbf{I} & -\mathbf{I} \\ & 16\mathbf{I} & 2\mathbf{I} \\ \mathbf{Sym.} & & 4\mathbf{I} \end{bmatrix},$$

$$\mathbf{K}_1^{(i)} = \frac{1}{30} h_i \begin{bmatrix} 4\mathbf{A}_1 & 2\mathbf{A}_1 & -\mathbf{A}_1 \\ & 16\mathbf{A}_1 & 2\mathbf{A}_1 \\ \mathbf{Sym.} & & 4\mathbf{A}_1 \end{bmatrix},$$

$$\mathbf{K}_4^{(i)} = \frac{1}{6} \begin{bmatrix} -6\mathbf{B}_4 + 3\mathbf{A}_4 & -4\mathbf{A}_4 & \mathbf{A}_4 \\ & 0 & -4\mathbf{A}_4 \\ \mathbf{Antisym.} & & 6\mathbf{B}_4 - 3\mathbf{A}_4 \end{bmatrix},$$

$$\mathbf{K}_6^{(i)} = \frac{1}{3 h_i} \begin{bmatrix} 7\mathbf{B}_6 & -8\mathbf{B}_6 & \mathbf{B}_6 \\ & 16\mathbf{B}_6 & -8\mathbf{B}_6 \\ \mathbf{Sym.} & & 7\mathbf{B}_6 \end{bmatrix},$$

in which $\mathbf{I}$ is a 2×2 identity matrix, and $\mathbf{A}_1$, $\mathbf{A}_4$, $\mathbf{B}_4$, and $\mathbf{B}_6$ are given by

$$\mathbf{A}_1 = \begin{bmatrix} c_{11} & 0 \\ 0 & c_{55} \end{bmatrix}, \quad \mathbf{A}_4 = \begin{bmatrix} 0 & c_{13} + c_{55} \\ c_{13} + c_{55} & 0 \end{bmatrix},$$

$$\mathbf{B}_4 = \begin{bmatrix} 0 & c_{55} \\ c_{13} & 0 \end{bmatrix}, \quad \mathbf{B}_6 = \begin{bmatrix} c_{55} & 0 \\ 0 & c_{33} \end{bmatrix},$$

where c_{ij} ($ij = 1,3,5$) are the stiffness matrix elements in (1) for the ith layer, and h_i and ρ_i are its thickness and mass density, respectively.

(2) The coefficients μ_{ij}, ν_i ($ij = 1,2$) in Eqs. (35a), (35b), (36a) and (36b) are given by

$$[\mu] = \frac{1}{D_{11} a^2 \omega^2} \begin{bmatrix} \lambda_1(i\kappa_1 a_1 - 1)/\kappa_1^2 & \lambda_1(i\kappa_1 a_1 + 1)/\kappa_1^2 \\ \lambda_2(i\hat{\kappa} a_1 - 1)/\hat{\kappa}^2 & \lambda_2(i\hat{\kappa} a_1 + 1)/\hat{\kappa}^2 \end{bmatrix},$$

$$[\nu] = \frac{1}{D_{11} a^2 \omega^2} [-\lambda_1 a_1^2/3 \quad -\lambda_2 a_1^2/3],$$

in which

$$\lambda_1 = \frac{2}{\eta \delta}, \quad \lambda_2 = \frac{c_0^2 \alpha^2 \eta}{2\delta},$$

$$\eta = \delta + (1/c_0^2 - 1/c_s^2)\omega, \quad \delta = \left[\left(\frac{1}{c_0^2} - \frac{1}{c_s^2} \right)^2 + \frac{4}{c_0^2 \alpha^2} \right]^{1/2},$$

where $\hat{\kappa} = -i\gamma$ for $|\omega| \leq \omega_c$ and $\hat{\kappa} = \kappa_2$ for $|\omega| > \omega_c$.

[1] K. F. Graff, *Wave Motion in Elastic Solids* (Clarendon, Oxford, England, 1975).
[2] J. Miklowitz, *Elastic Waves and Waveguides* (North-Holland, Amsterdam, 1978).
[3] S. K. Datta, J. D. Achenbach, and Y. S. Rajapakse, *Elastic Waves and Ultrasonic Nondestructive Evaluation* (North-Holland, Amsterdam, 1990).
[4] A. N. Ceranoglu and Y. H. Pao, ''Propagation of elastic pulses and acoustic emission in a plate, part 1: theory,'' J. Appl. Mech. **48**, 125–132 (1981).
[5] A. N. Ceranoglu and Y. H. Pao, ''Propagation of elastic pulses and acoustic emission in a plate, part 2: epicentral responses,'' J. Appl. Mech. **48**, 133–138 (1981).
[6] A. N. Ceranoglu and Y. H. Pao, ''Propagation of elastic pulses and acoustic emission in a plate, part 3: general responses,'' J. Appl. Mech. **48**, 139–147 (1981).
[7] A. K. Mal and S. S. Lih, ''Elastodynamic response of a unidirectional composite laminate to concentrated surface loads: part I,'' J. Appl. Mech. **59**, 878–886 (1992).
[8] S. S. Lih and A. K. Mal, ''Elastodynamic response of a unidirectional composite laminate to concentrated surface loads: part II,'' J. Appl. Mech. **59**, 887–892 (1992).
[9] I. Tolstoy and E. Usdin, ''Wave propagation in elastic plates: low and high mode dispersion,'' J. Acoust. Soc. Am. **29**, 37–42 (1957).
[10] A. H. Meitzler, ''Backward-wave transmission of stress pulses in elastic cylinders and plates,'' J. Acoust. Soc. Am. **38**, 835–842 (1965).
[11] P. J. Torvik, ''Reflection of wave trains in semi-infinite plates,'' J. Acoust. Soc. Am. **41**, 346–353 (1967).
[12] S. B. Dong and R. B. Nelson, ''On natural vibrations and waves in laminated orthotropic plates,'' J. Appl. Mech. **39**, 739–745 (1972).
[13] S. B. Dong and K. H. Huang, ''Edge vibrations in laminated composite plates,'' J. Appl. Mech. **52**, 433–438 (1985).
[14] W. Karunasena, A. H. Shah, and S. K. Datta, ''Wave propagation in a

multilayered laminated cross-ply composite plate,'' J. Appl. Mech. **58**, 1028–1032 (1991).

[15] K. Kausel, ''Wave propagation in anisotropic layered media,'' Int. J. Numer. Methods Eng. **23**, 1567–1578 (1986).

[16] J. L. Rose, J. J. Ditri, and A. Pilarski, ''Wave mechanics in acousto-ultrasonic nondestructive evaluation,'' J. Acoust. Emiss. **12**, 23–26 (1994).

[17] S. Pelts and J. L. Rose, ''Source influences on elastic guided waves in an orthotropic plate,'' J. Acoust. Soc. Am. **99**, 2124–2129 (1994).

[18] G. R. Liu, J. Tani, T. Ohyoshi, and K. Watanabe, ''Transient waves in anisotropic laminated plates, part I: theory,'' Trans. ASME, J. Vib. Acoust. **113**, 230–234 (1991).

[19] R. V. Churchill and J. W. Brown, *Complex Variables and Applications* (McGraw–Hill, New York, 1990).

[20] M. Veidt and W. Sachse, ''Ultrasonic evaluation of thin, fiber-reinforced laminates,'' J. Compos. Mater. **28**, 329–342 (1993).